

# Green Synthesis of Gold Nanoparticles, Silver Nanoparticles and Gold-Silver Alloy Nanoparticles Using *Ziziphus spina-christi* Leaf Extracts and Antibacterial Activity against Multidrug-Resistant Bacteria

SEHAM ALZHRANI<sup>1,2\*</sup>, H. M. ALI<sup>1</sup>, EMAN HILLAL ALTHUBAITI<sup>2</sup> AND M. M. AHMED<sup>1,3</sup>

Department of Biology, <sup>1</sup>Department of Biological Sciences, College of Science, King Abdulaziz University, Jeddah, 21589, <sup>2</sup>Department of Biotechnology, College of Science, Taif University, Taif 21944, Saudi Arabia, <sup>3</sup>Nucleic Acids Research Department, Genetic Engineering and Biotechnology Research Institute, The City of Scientific Research and Technological Applications, Alexandria 21548, Egypt

## Alzahrani *et al.*: Synthesis of Nanoparticles Using *Ziziphus spina-christi* Leaf Extracts and its Antibacterial Activity

Multidrug-resistant bacteria continue to pose the greatest threat to public health. Metallic nanoparticles are one of the more promising strategies for combating antibiotic resistance. This research aims to determine the effect of gold and silver nanoparticles and gold-silver alloy nanoparticles as antibacterial agents. On the other hand, biogenic synthesized gold and silver nanoparticles using *Ziziphus spina-christi* leaf extract and preparation of gold-silver alloy nanoparticles for treatment of multidrug-resistant bacteria were studied. The formation of nanoparticles was characterized using ultraviolet-visible spectrophotometer, fourier transforms infrared spectroscopy, X-ray diffraction and transmission electron microscopy. Antibacterial activity of the biosynthesized gold nanoparticles, silver nanoparticles and gold-silver alloy nanoparticles was studied against *Klebsiella pneumoniae*, *Escherichia coli*, *Pseudomonas aeruginosa*, *Staphylococcus aureus*, *Acinetobacter baumannii* and *Enterococcus faecalis*. In the present study, the minimum inhibitory concentration ranged from 61.33 to 64 µg/ml and the minimum bactericidal concentration of the silver nanoparticles ranged from 85.33 to 93.33 µg/ml against multidrug-resistant strains. Synthesized gold nanoparticles had no inhibition zone, indicating that silver nanoparticles have no negative effect on multidrug-resistant bacteria. Minimum inhibitory concentration of gold nanoparticles was in high concentration against multidrug-resistant strain was not bactericidal. The highest minimum inhibitory concentration of gold nanoparticles was 114 µg/ml. Finally, the minimum inhibitory concentration ranged from 53.33 to 62 µg/ml and the minimum bactericidal concentration of the gold-silver alloy nanoparticles ranged from 77.33 to 93.33 µg/ml against multidrug-resistant strains. These results indicate that gold-silver alloy nanoparticles showed higher antimicrobial ability when compared to silver nanoparticles and gold nanoparticles alone. Finally, the synthesized nanoparticles could be used as an alternative antimicrobial agent against multidrug-resistant bacteria, according to our findings.

**Key words:** Silver nanoparticles, gold nanoparticles, multidrug-resistant bacteria, metallic nanoparticles

Since the beginning of nanotechnology, various Nanoparticles (NPs) synthesis methods have been observed and changed for the better. Many of these processes use hazardous chemicals, much energy and much heat to create NPs with limited properties. Green synthesis methods based on a microwave, sonochemical, electrochemical and hydrothermal methods, for example, have been developed to address this problem.

Green synthesis methods that use biological material sources such as plants, microbes and agricultural and industrial wastes have recently gained traction<sup>[1]</sup>. To a large extent, biological synthesis has been used to produce NPs of bimetallic or trimetallic alloys<sup>[2]</sup>.

Silver (Ag) is a flexible, stronger than Gold (Au) natural element that is also a great insulator of thermal and electric energy<sup>[3]</sup>. Silver Nanoparticles (AgNPs)

\*Address for correspondence

E-mail: seham.alzahrani@hotmail.com

and their variants have a long history of medical applications<sup>[4]</sup>. Many studies have found a connection between AgNPs bactericidal activity and their ability to penetrate bacterial cell walls and alter membrane structure. Unchecked movement through the cell membrane and the eventual death of the bacteria result from this alteration in cell permeability. Other studies relate antimicrobial property to the generation of free radicals that damage membranes<sup>[5]</sup>. Researchers have discovered that the enzyme-activating thiol groups interact with AgNPs, which in turn prevents enzyme activation and cell division<sup>[6]</sup>. Another mechanism by which Ag ions are thought to interfere with protein translation is their binding to the ribosomal subunit 30S.

Aqueous solutions of Au contain no free ions because it is rigid and rare metal. Gold Nanoparticles (AuNPs) are non-toxic to human cells. AuNPs bactericidal activity does not promote the formation of Reactive Oxygen Species (ROS), which are the primary cause of bacterial cell death and this, is why they are effective against bacteria<sup>[7]</sup>. It has been found that AuNPs have no effect on bacterial growth or activity, but vancomycin-AuNPs conjugates reduce the number of growing bacterial cells. The antibacterial properties of vancomycin-coated stable AuNPs were of considerable rise when compared to that of the free antibiotics<sup>[8]</sup>.

Alloy NPs are made up of two or more metals that have properties like hardness, strength and durability in a homogeneous mixture<sup>[9]</sup>. For various applications, such as incorporating AgNPs with AuNPs, NPs must be combined with other materials. Due to this incorporation, their properties differ from those of monometallic NPs, such as the ability to catalyze, which is higher in alloy NPs than in monometallic NPs<sup>[10]</sup>. Alloy compounds have different structures and physical properties than their parent elements and possess superior characteristics to those of their parent elements. AgNPs-AuNPs, AgNPs-Copper Nanoparticles (CuNPs), AgNPs-Titanium Dioxide Nanoparticles (TiNPs) and AuNPs-Palladium Nanoparticles (PdNPs) are the most well-known bimetallic NPs. Optical, catalytic and electronic properties make them excellent choice bimetallic NPs are preferable to monometallic NPs. Grade *et al.* studies of the bactericidal effect of AgNPs-AuNPs alloy NPs on *Staphylococcus aureus* (*S. aureus*) using laser ablation drew more attention to the possibility of a new medical treatment field<sup>[11]</sup>. With the help of dextran solution, Dos Santos *et al.* synthesized an Ag-Au alloy with significant antimicrobial properties against a wide variety of biological growth, which could be used in

medical equipment and antimicrobial agents<sup>[12]</sup>.

AgNPs and AuNPs with desired morphology and size have been prepared using natural capping, reducing and stabilizing agents using green chemistry methods in recent years. Metallic Nanoparticles (MNPs) can be synthesized using biological methods rather than toxic, harsh and expensive chemical substances. Metal ion bioreduction is a chemically complex but environmentally friendly process that uses polysaccharides, proteins and vitamins which are examples of biomolecules that can be found in certain organisms extracts. The most common method for producing green NPs is the use of plant extracts to synthesize MNPs. Furthermore, the plants have the distinct advantage of being widely distributed, readily available, much safer to handle, low cost, simple to scale up for huge synthesis and do not require the use of toxic chemicals, high pressure, temperature or energy and act as a source of several metabolites, as well as being a source of several metabolites<sup>[13]</sup>.

*Zizyphus spina-christi* (*Z. spina-christi*) is a member of the Rhamnaceae family, which includes plants native to tropical Africa and Asia. Traditional medicine uses *Z. spina-christi* to treat inflammatory and pain-related ailments in areas where the plant is found. A local application of wood ash mixed with vinegar is recommended in the treatment of serpent bites. Fresh green leaf cataplasm is applied to swollen eyes before going to bed for abscesses and furuncles. Fruit infusions have been used to treat measles because they are emollients and laxatives<sup>[14]</sup>. *Z. spina-christi* leaf extract phytochemical analyses revealed the presence of phenolic, flavonoids, tannins, alkaloids and saponins. Because of the high concentration of Hydroxyl (OH)-groups in *Z. spina-christi* phytochemical compounds, these antibacterial and antioxidant properties are enhanced<sup>[15]</sup>.

The emergence of Multidrug-Resistant (MDR) bacteria is a significant public health issue, necessitating the creation of new bactericidal materials. Many antimicrobial drugs face a major challenge because of pathogens acquired resistance<sup>[16]</sup>. Over 70 % of bacteria that cause infections in hospitals are resistant to at least one antibiotic, according to the World Health Organization (WHO) and some species are resistant to all approved antibiotics. The MDR isolates of *S. aureus*, *Klebsiella pneumoniae* (*K. pneumoniae*), *Pseudomonas aeruginosa* (*P. aeruginosa*), *Enterococcus faecium* (*E. faecium*), *Enterobacter species* and *Acinetobacter baumannii* (*A. baumannii*) cause 16 % of all healthcare-

associated infections, putting healthcare professionals on the defensive<sup>[17]</sup>. Bacteria are able to adapt to the selection pressure of antibiotics, resulting in their ability to develop and maintain antibiotic resistance. In addition, the variety of mechanisms for antibiotic resistance has risen in recent years<sup>[18]</sup>.

*Z. spina-christi* extracts were used as a reducing and stabilizing agent for the biosynthesis of Au, Ag and Au-Ag alloy NPs in this study. AgNPs combined with *Z. spina-christi* leaf extract had a synergistic bactericidal effect on the biosynthesized Au-Ag alloy NPs. As an alternative to conventional antibacterial materials, this hybrid nanomaterial has been developed.

## MATERIALS AND METHODS

### Plant collection and preparation of extract:

Fresh *Z. spina-christi* leaves were collected in the Al Shafa area of Taif, Saudi Arabia, during the summer. To make fresh aqueous extract plants, for 30 min at 80°, 25 g of thoroughly cleaned and finely chopped plants were sterilized in 100 ml of double-distilled water. The extract was filtered through Whatman filter paper no. 1 and kept at 4° for up to 1 w (fig. 1).

### Biosynthesis of NPs using plant extract:

**AgNPs biosynthesis:** 1 ml of the prepared plant extract was added to 10 ml of 1 mM Silver Nitrate (AgNO<sub>3</sub>) with constant stirring at room temperature<sup>[19]</sup>. During exposure to plant extracts, Ag ions were reduced into AgNPs, resulting in the color change.

**AuNPs biosynthesis:** The *Z. spina-christi* extract (1 ml) was added to 25 ml of 1 mM Chloroauric Acid (HAuCl<sub>4</sub>) at room temperature for 20 min<sup>[20]</sup>. NPs had formed when the color of the solution changed from light yellow to red grape.

### Biosynthesis of Au-Ag alloy NPs:

For Au-Ag alloys NPs synthesis, at room temperature, in 25 ml of deionized water, 1 mM AgNO<sub>3</sub> and 1 mM HAuCl<sub>4</sub> were dissolved. At a rate of 10 min, the reaction solution was heated to 90° while being stirred at 600 rpm. The solution was then injected with 25 ml *Z. spina-christi* extract. The solution was kept at 90° for 3 h before cooling to room temperature. The reaction mixture changed color from yellow to dark due to Au-Ag alloys<sup>[21]</sup>.

### Characterization of NPs:

**Ultraviolet-Visible (UV-Vis) spectra:** The formation of AuNPs, AgNPs and Au-Ag alloys was monitored using double-beam spectrophotometry using *Z. spina-christi* leaf extract at a resolution of 1 nm in the 300-800 nm wavelength range<sup>[22]</sup>.

**Transmission Electron Microscopy (TEM):** The microscopy technique known as TEM (Hitachi, H-7500) involves passing an electron beam through an ultra-thin specimen and interacting with it as it passes through. These NPs images of AuNPs, AgNPs and Au-Ag alloys NPs are the result of electrons passing through the specimen, which are magnified and focused on an imaging device<sup>[23]</sup>.

**X-Ray Diffraction (XRD) analysis:** AuNPs, AgNPs and Au-Ag alloys NPs were examined using XRD to figure out their particle size and chemical composition. With 30 kV, 30 mA and Cu K radiations at an angle of 2θ, the Shimadzu XRD-6100/6100 model was used. After the material was finely ground, the bulk composition of the analyzed material was determined. For the AgNPs and AuNPs, Debye Scherer's equation was used to determine the particle or grain size<sup>[24]</sup>.

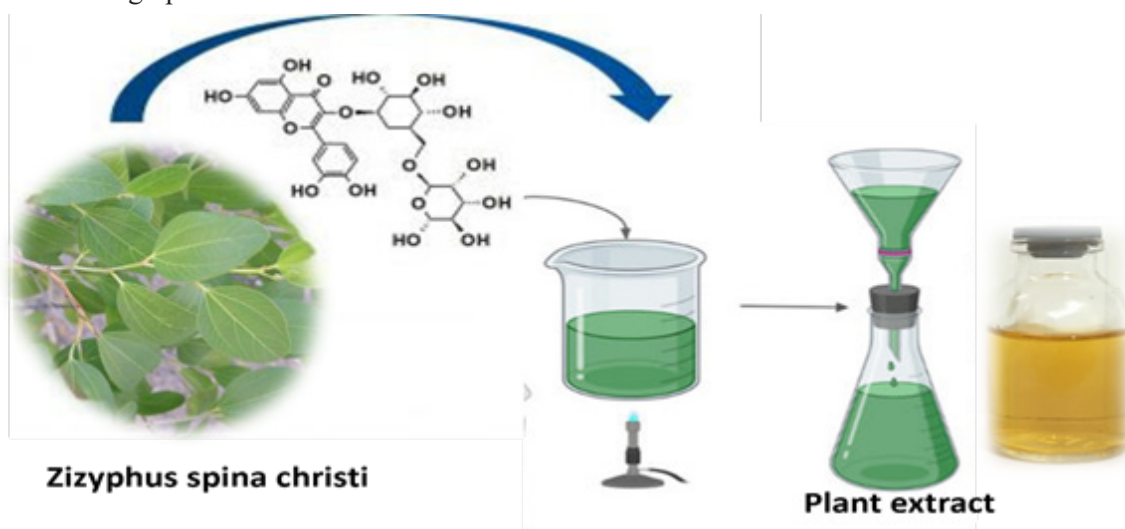


Fig. 1: *Z. spina-christi* leaf extracts preparation

### Fourier Transform Infrared Spectroscopy (FTIR):

To remove any loose moieties, centrifuge at 10 000 g for 20 min, the stabilized AuNPs, AgNPs and Au-Ag alloys solution was collected and dried thoroughly. The Shimadzu IR-470 spectrometer was used to conduct FTIR measurements on the AuNPs, AgNPs and Au-Ag alloys powder (Shimadzu, Japan). It has been determined that the FTIR peaks of the AuNPs and AgNPs were identified and expressed in wavenumbers ( $\text{cm}^{-1}$ ). A leaf extract from *Z. spina-christi* was also examined<sup>[25]</sup>.

### Characterization and isolation:

Clinical isolates collection and growth conditions: Urine and sputum specimens were collected from King Faisal Hospital, Taif, Saudi Arabia. For 24-48 h, the bacteria were incubated at 37° on Cystine Lactose Electrolyte Deficient (CLED) agar, Blood agar and MacConkey agar. Based on the colony morphology on blood and MacConkey agar, Gram-negative bacteria were identified through biochemical reactions like those for oxidase, Sulfide Indole Motility (SIM), Triple Sugar Iron (TSI), citrate and urease<sup>[26]</sup>. *K. pneumoniae*, *Escherichia coli* (*E. coli*), *P. aeruginosa*, *S. aureus*, *A. baumannii* and *E. faecalis* were found to be the most common bacterial isolates found in the samples. These bacterial strains were kept on Mueller-Hinton agar slants in the clinical laboratories during the antimicrobial efficacy study at a temperature of 4° to maintain viability. At a temperature of 37°, bacteria were subcultured in Mueller-Hinton broth. 10<sup>7</sup> Colony-Forming Unit (CFU)/ml was the final concentration of the cell suspensions after diluting them with sterile saline solution, further efficacy of antimicrobials studies were carried out using AuNPs, AgNPs and Au-Ag alloys to investigate their antimicrobial properties.

**Susceptibility testing for antibiotics:** The Kirby-Bauer disc diffusion method on Mueller-Hinton agar was used to test bacterial isolates for antibiotic susceptibility according to Clinical and Laboratory Standards Institute (CLSI) guidelines<sup>[27]</sup>. 0.5 McFarland turbidity standards were used to grow it at 37°. Discs of antibiotics were added to a Mueller-Hinton agar plate for the bacterial culture. The CLSI guidelines were used to interpret the Zone of Inhibition (ZIN) on the plates after an overnight incubation period.

**Antibacterial activity of AuNPs, AgNPs and Au-Ag alloys using agar diffusion method:** This procedure was used to test the antimicrobial properties of the metal NPs against MDR bacteria<sup>[28]</sup>. The nutrient broth was used to grow the MDR bacteria at 37° overnight

and grown MDR bacteria were then again subcultured into nutrient broth media and allowed to grow for another 2 h until the Optical Density (OD) was reduced to 0.01. On nutrient agar plates, 100 l of liquid culture were evenly distributed. An agar well borer was used to create wells with a diameter of 6 mm on agar plates and incubated at 37° with the AuNPs, AgNPs and Au-Ag alloys in the wells. The diameter of bacterial clearance after 16-24 h was used to calculate the ZIN.

### Micro-dilution test for Minimum Inhibitory Concentration (MIC) and Minimum Bactericidal Concentration (MBC) determination:

The test was carried out by inoculating bacterial culture into the wells of a microdilution plate and arranging antibiotic dilutions across the rows. Dilution tests can also be performed using individual tubes or plates in modern laboratories, but high-throughput plates were used in this experiment. A series of dilutions of antibiotic drug concentrations, with each concentration in a range being doubled from lowest to highest, were used to test for antibiotic efficacy. An *in vitro* test of the drug's activity and bacterial resistance was required for the MIC to be helpful. Drug-resistant isolates have a lower MIC value. The MICs were calculated using serial two-fold dilutions of AgNPs ranging from 96  $\mu\text{g/ml}$  to 8  $\mu\text{g/ml}$  and AuNPs ranging from 114  $\mu\text{g/ml}$  to 8  $\mu\text{g/ml}$ . The concentrations are always given in  $\mu\text{g/ml}$ . MBC is the lowest concentration that can kill 99.9 % of microorganisms<sup>[29]</sup>. MBC is possible, but it is more complex than determining MIC. As a result, clinical laboratories rarely measure or report the MBC<sup>[30]</sup>.

### Statistical analysis:

Each activity assay was performed in triplicates. One-way Analysis of Variance (ANOVA) in Statistical Package for the Social Sciences (SPSS) statistics program (IBM SPSS statistics 22) was used to evaluate the significance levels of results at  $p < 0.05$ .

## RESULTS AND DISCUSSION

$\text{AgNO}_3$  (1 mM) and *Z. spina-christi* leaf extract (25 %) were used to create AgNPs, which led to a color shift from yellow to brown, then dark brown, as depicted in the image above (fig. 2). AgNPs, which are formed when Ag salt is reduced, were responsible for the solution's color change. Reducing and stabilizing agents allowed Ag ions to be reduced to AgNPs. The excitation of surface plasmon vibrations caused the yellowish-brown color of AgNPs in an aqueous solution. The color of the reaction mixture remained the same for about an hour after the color change was complete. So the reaction

mixture's  $\text{AgNO}_3$  concentration had been reduced drastically.

Our findings corroborate those of SP *et al.*<sup>[31]</sup>. First, the absorption spectrum was produced by strong Surface Plasmon Resonance (SPR) or the resonant absorption of photons by AgNPs. Because the SPR band was affected by the refractive index of the solution and the size, the observed absorption band was size-dependent<sup>[32]</sup>. SPR of metal UV-Vis spectrometry that AgNPs are being formed has been confirmed, which revealed a sharp peak at 420 nm (fig. 3)<sup>[33]</sup>.

Fig. 4 shows that within 30 min of the Au salt solution's addition to plant extract, the extracts color changed from colorless to wine red, indicating that AuNPs had formed. This is due to the molecular assistance of biological reducing agents found in the plant extract in the fabrication of AuNPs. The presence of reducing agents caused Au ions to be reduced to AuNPs. Natural

reducing agents were found in *Z. spina-christi* leaf extract, which converted aqueous  $\text{HAuCl}_4$  solution to AuNPs. Due to the excitation of SPR, AuNPs showed a red grape color in an aqueous solution and showed a sharp peak at 550 nm (fig. 3)<sup>[34]</sup>. The observed absorption band was influenced by the solution's size and refractive index, making the SPR band size-dependent<sup>[35]</sup>.

*Z. spina-christi* was used to successfully synthesize metallic NPs of Au, Ag and Au-Ag alloys NPs. Deionized water was used to dissolve 1 mM  $\text{AgNO}_3$  and 1 mM  $\text{HAuCl}_4$  in 25 ml. Following that, the reaction solution was brought to  $90^\circ$  by stirring it at 600 rpm for 10 min at a time. The solution was then injected with 25 ml *Z. spina-christi* extract. Before allowing the solution to cool to room temperature, it was kept at  $90^\circ$  for 3 h. Au-Ag alloys were formed and the reaction mixture turned dark yellow<sup>[35]</sup>. A UV-Vis spectrophotometer confirmed the formation of these MNPs (fig. 5).

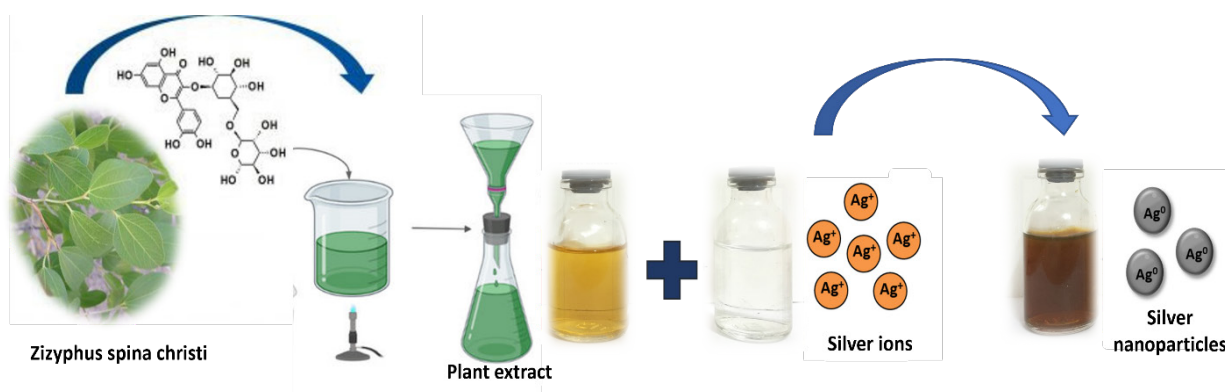


Fig. 2: *Z. spina-christi* leaf extract solution changes color over time when  $\text{AgNO}_3$  is added to it

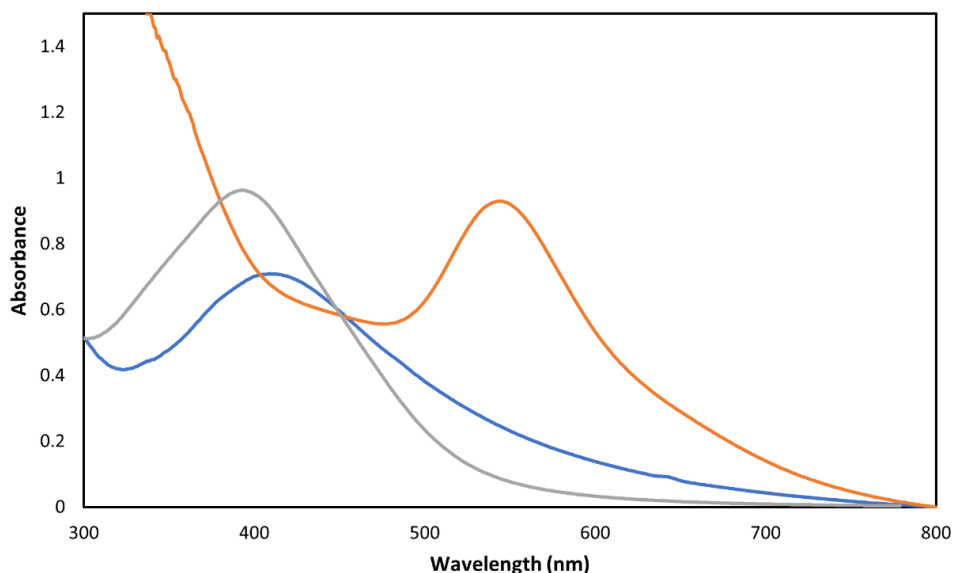


Fig. 3: AuNPs, AgNPs and Au-Ag alloys NPs UV-Vis spectra using *Z. spina-christi* leaf extract, (—) Au-Ag alloy; (—) Au; (—) Ag

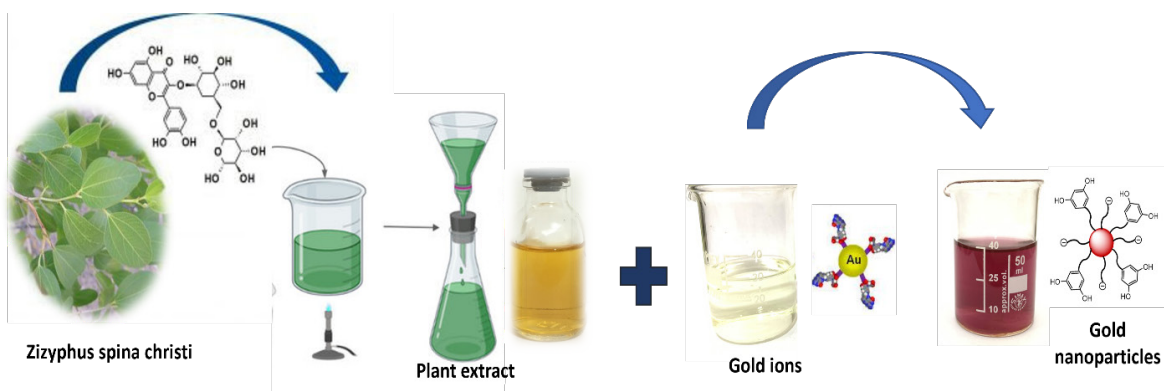


Fig. 4: The color of the solution changes over time by adding  $\text{HAuCl}_4$  to *Z. spina-christi* leaf extract



Fig. 5: Biosynthesis of Au-Ag alloys NPs

UV-Vis spectroscopy of AuNPs, AgNPs and Au-Ag alloys NPs was described below. The most common bimetallic NPs structures are alloys and core-shells, following the atoms intrinsic properties and their synthesis techniques. A structure can be determined by using the UV-Vis spectroscopy technique. SPR bands have been discovered in AuNPs and AgNPs, for example. For core-shell NPs, metal clusters separated into cores and shells typically show two distinct peaks in absorbance. Pure NPs have two absorption peaks, but the alloy NPs has a single absorption peak in the middle. Figure depicting each product's UV-Vis spectra are shown (fig. 3). There was only one absorption peak between 413 and 545 nm in all samples (Ag or Au NPs). When the metal precursor's mole fraction of Au reaches 50 % (i.e., the Au/Ag ratio is 1:1), an SPR peak appears at 425 nm.

A single SPR peak shift from AuNPs and AgNPs can be used to identify Au-Ag alloy NPs. For the bi-metallic alloy, a single SPR peak is expected, whereas two SPR peaks are expected if two individual metal NPs are physically mixed in the same condition. In a previous study, a shift in the SPR peak was observed<sup>[36]</sup> and other reports<sup>[37]</sup> for obtaining Au-Ag alloy NPs using

*Jasminum sambac* (*J. sambac*) and *Fusarium semicatum* (*F. semicatum*) fungi extracts, respectively<sup>[38]</sup>.

High-resolution TEM was used to examine the size and morphology of biosynthesized AgNPs with sizes ranging from 11.9 to 38.8 nm and a scale of 20 nm, as well as a histogram showing sizes of particles with spherical and hexagonal morphology<sup>[39]</sup>. TEM micrograph indicates the AuNPs were spherical and hexagonal (fig. 6). The synthesized AuNPs were formed in 14.64-32.95 nm in size. Our results were correlated to data obtained by Patil *et al.*<sup>[40]</sup>. The particles in the biosynthesized Au-Ag alloy were spherical and hexagonal, with an average size of 12.62-40.62 nm, according to TEM images (fig. 6)<sup>[41]</sup> diameter on average of 15 nm was found for individual AgNPs and AuNPs, suggesting that electron densities within the particle volume were more uniform. AgNPs were more dispersed than AuNPs, which were more aggregated and Au-Ag alloy.

Au, Ag and Au-Ag alloy FTIR spectra are depicted in fig. 7. Identification of bioactive molecules for the stability of future generations of NPs through the reduction and bio-capping of MNPs was carried out using FTIR.

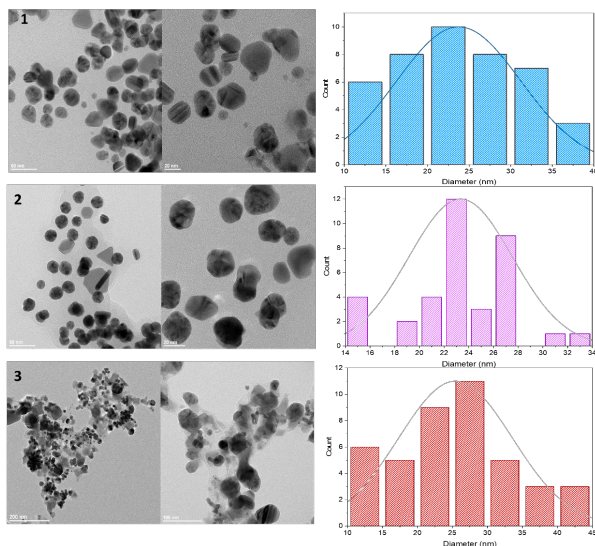


**Fig. 6:** TEM images of biosynthesized, (1) AgNPs; (2) AuNPs and (3) Au-Ag alloy NPs with corresponding particle size distribution histograms

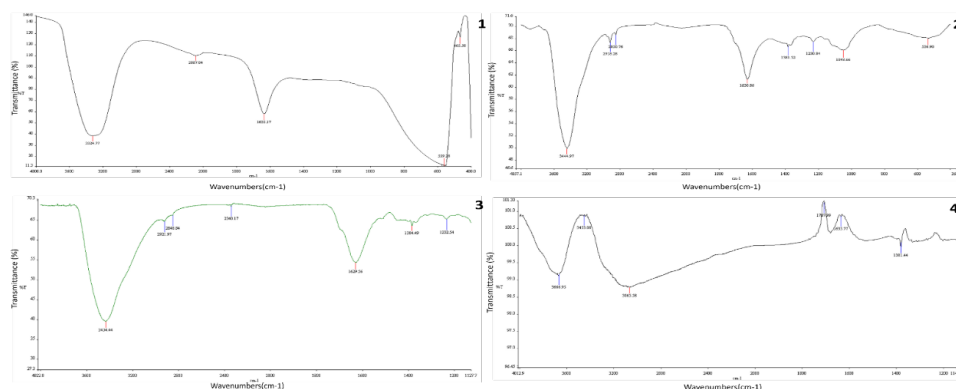


**Fig. 7:** FTIR spectra of biosynthesized, (1) Extract; (2) AgNPs; (3) AuNPs and (4) Au-Ag alloy NPs

The FTIR analysis of AgNPs revealed two sharp absorption peaks at  $1630\text{ cm}^{-1}$  and  $3444\text{ cm}^{-1}$ , indicating possible protein-AgNPs interaction. This peak, which corresponded to OH stretching or H-bonding for alcohol or phenols, was found at  $3324\text{ cm}^{-1}$ , indicating that OH bonding is enhanced during the formation of NPs. The amine peak was between  $1630$  and  $1633\text{ cm}^{-1}$ . The absorption peak of  $1635.89\text{ cm}^{-1}$  is similar to that of proteins<sup>[42]</sup>.

The above-mentioned functional groups are mostly derived from heterocyclic compounds, as indicated by the FTIR data and these are the water-soluble components of *Z. spina-christi*. As a result, water-soluble compounds like phenolic, alcohol and amines may act as capping agents in the synthesis of AuNPs, as well as aiding in NPs stabilization under physiological conditions. The capping and stabilization of AuNPs have been attributed to hydroxyl groups and amines<sup>[43]</sup>.

To the presently formed phyto-mediated NPs, an FTIR analysis was performed. The active biomolecules found in plant leaves include amides, hydroxyls, ketones, ethers, alkyls and other functional groups that have previously been reported<sup>[44]</sup>. The FTIR spectra of AuNPs, AgNPs and Ag-Au NPs have been published and possible peaks from the biomolecules responsible for photosynthesized NPs reduction, capping and efficient stabilization have been identified.

According to the FTIR data, the different functional groups mentioned above are mostly derived from heterocyclic compounds and these are the water-soluble components of *Z. spina-christi*. As a result, water-soluble compounds such as phenolic, alcohol and amines may act as a capping agent in the synthesis of AuNPs, aiding in NPs stabilization under physiological conditions. Hydroxyl groups and amines are thought to be responsible for the capping and stabilization of AuNPs<sup>[45]</sup>.

Fig. 8 shows the Au, Ag and Au-Ag alloy NPs synthesized in a biosynthetic manner. As metals with similar lattice constants, the two values of Au-Ag alloys are very close. The four intense peaks are found at  $2\theta=37.51^\circ$ ,  $44.12^\circ$ ,  $64.00^\circ$  and  $76.91^\circ$ , which correspond to (111), (200), (220) and (311), respectively and can be indexed using the facets of AuNPs and AgNPs face-centered cubic crystal structure. The bimetallic Au-Ag alloys reflections are identical to the monometallic Au and Ag NPs. Using the Scherrer equation, the mean sizes of these NPs were calculated to be 2430 nm based on the line width of the maximum intensity reflecting peak.

The Debye-Scherrer formula is used to calculate the average crystalline size.

$$D=K\lambda/\beta \cos \theta$$

Where K is Scherrer constant,  $\lambda$  is the wavelength of X-ray,  $\theta$  is the Bragg's angle in radians and beta ( $\beta$ ) is the full width at half maximum of the peak in radians.

A geometric factor of (0.9), the XRD source's wavelength and the angular Full-Width at Half Maximum (FWHM) of the XRD peak at the angle

of diffraction  $\theta$  are used to calculate D, the average crystalline size of NPs (fig. 8).

In our results of the XRD spectrum of the biosynthesized NPs, the D and  $2\theta$  values of Au and Ag NPs have similar lattice constants. Au-Ag alloys are very similar. However, the four intense peaks are observed at  $2\theta=37.51^\circ$ ,  $44.12^\circ$ ,  $64.00^\circ$  and  $76.91^\circ$  corresponding to (111), (200), (220) and (311), which can be indexed according to the facets of the face-centered cubic crystal structure of Au and Ag NPs<sup>[46]</sup>. The Au-Ag alloy's reflections are identical to the monometallic NPs of Au and Ag. Based on the line width of the maximum intensity reflecting peak, the mean sizes of these NPs were calculated to be 25-30 nm using the Scherrer equation<sup>[38]</sup>.

The bacterial strains *K. pneumoniae*, *E. coli*, *P. aeruginosa*, *S. aureus*, *A. baumannii*, *E. faecalis* were isolated from urine and sputum. Antimicrobial agent sensitivity testing was performed on the bacterial isolates found in urine and sputum. The antimicrobial MICs of these bacterial strains were tested against each other (Table 1).

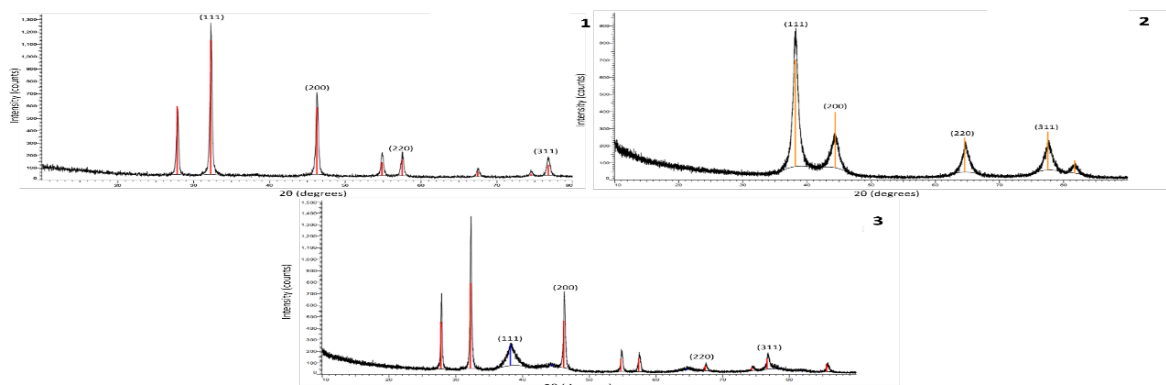


Fig. 8: XRD analysis of biosynthesized, (1) AgNPs, (■) Ag ; (2) AuNPs, (■) Au; (3) Au-Ag alloy NPs, (■) AgNPs and (■) AuNPs

TABLE 1: PATTERNS OF RESISTANCE TO MDR BACTERIA FOUND IN URINE AND SPUTUM ISOLATES

Bacterial isolates	Antibiotic resistance pattern	Number of antibiotics	Sources
<i>K. pneumoniae</i>	AK, AMP, AMC, ATM, FEP, FOX, CAZ, CRO, CXM, CEF, CIP, ETP, GEM, IPM, LVX, MEM, NTF, TZP, SXT	19	Urine
<i>E. coli</i>	AK, AMP, ATM, FEP, CAZ, CRO, CXM, CEF, CIP, GEM, LVX, SXT	12	Urine
<i>P. aeruginosa</i>	AK, AMP, AMC, ATM, FEP, FOX, CAZ, CRO, CXM, CEF, CIP, ETP, GEM, IPM, LVX, MEM, NTF, TGC, SXT	19	Urine
<i>S. aureus</i>	AMP, ATM, CTX, CEC, GEM, IPM, CIP, OXA, PEN	9	Sputum
<i>A. baumannii</i>	AK, AMP, AMC, ATM, FEP, FOX, CAZ, CRO, CXM, CEF, CIP, ETP, GEM, IPM, LVX, MEM, NTF, TZP, SXT	19	Sputum
<i>E. faecalis</i>	CTX, FOX, CEC, CLI, ERY, GEM, IPM, CIP, TET, SXT	10	Urine

Note: AMC:Amoxy/Clavulanic acid; CTX: Cefotaxime; FOX: Cefoxitin; LVX: Levofloxacin; CRO: Ceftriaxone; CIP: Ciprofloxacin; AMP: Ampicillin; LEX: Cefalexin; FEP: Cefepim; MEM: Meropenem; CAZ: Ceftazidime; SXT: Sulpha/Trimethoprim; CXM: Cefuroxime; GEM: Gentamicin; IPM: Imipenem; ATM: Aztreonam; CEF: Cephalothin; ETP: Ertapenem; NIT: Nitrofurantoin; TGC: Tigecycline; IPM: Imipenem; TZP: Piperacillin-tazobactam; CLI: Clindamycin; AK: Amikacin; DAP: Daptomycin; ERY: Erythromycin; FUS: Fusidic acid; CEC: Cefaclor; LZD: Linezolid; MXF: Moxifloxacin; MUP: Mupirocin; NTF: Nitrofurantoin; OXA: Oxacillin; FEP: Cefepime; PEN: Penicillin G; RIF: Rifampicin; TEC: Teicoplanin; TET: Tetracycline and VAN: Vancomycin

The results obtained have been interpreted following the CLSI guidelines. First, as presented in Table 1, the isolates of *K. pneumoniae* were resistant to 19 antimicrobials and isolates of *E. coli* were resistant to 12. Moreover, isolate *P. aeruginosa* was resistant to 19 antibiotics and isolates *S. aureus* was resistant to 9. Also, isolate *A. baumannii* was resistant to 19 antibiotics and isolates *E. faecalis* was resistant to 10. According to Matsushita and Janda<sup>[47]</sup>, many bacterial strains have mobile components that encode antibiotic resistance and can be transferred between them or even between different species by horizontal or vertical gene transfer. Other mechanisms of resistance could be caused by chromosomal Deoxyribonucleic Acid (DNA) mutation. According to the findings, bacteria's rapid growth rate and the absolute number of cells reached mean, that resistance develops quickly in a population with high infection rates<sup>[47]</sup>. The antibiogram of these isolates showed high resistance rates to critically essential antibiotics, which WHO classifies, making these infections hard to treat by many classes of antibiotics ( $\beta$ -lactamase, cephalosporins, aminoglycosides, fluoroquinolones and lincosamides)<sup>[48]</sup>.

*K. pneumoniae*, the most common cause of nosocomial infection-related mortality and morbidity, has a high rate of resistance that can spread into the general population, making treatment more difficult<sup>[49]</sup>. The findings revealed high levels of resistance to commonly used antimicrobials. Mutations that alter the expression and function of chromosomally encoded mechanisms can lead to antibacterial resistance in *P. aeruginosa*; alternatively, the bacteria can acquire resistance genes on mobile genetic elements (plasmids)<sup>[50]</sup>. Extended Spectrum Beta-Lactamase (ESBLs) or AmpC-type cephalosporins and uncommon carbapenemases, which are plasmid and integron-mediated antimicrobial resistance determinants, are commonly produced by MDR strains of *A. baumannii*<sup>[51]</sup>. Their prevalence is relatively high in some settings<sup>[52]</sup>.

Micro-dilution plates and a suitable diffusion assay are used. The antibacterial properties of synthesized NPs were tested against several MDR bacterial pathogens. ZIN, MIC and MBC are the diameters of the ZIN in millimeters (Table 2, Table 3 and fig. 9).

**TABLE 2: BIOSYNTHESIZED Au, Ag AND Au-Ag ALLOY NPs HAVE ANTIBACTERIAL PROPERTIES AGAINST MDR PATHOGENIC STRAINS WAS COMPARED TO THAT OF A STANDARD DRUG**

Test Samples	Mean ZIN (mm) (Mean $\pm$ SD)			
	Au NPs	Ag NPs	Au-Ag NPs	Standard (Cefepime)
Concentration ( $\mu$ g/ml)	100	100	100	20
<i>K. pneumoniae</i>	00.00 $\pm$ 0.00	14.67 $\pm$ 0.58	15.67 $\pm$ 0.58	17.33 $\pm$ 0.58
<i>E. coli</i>	00.00 $\pm$ 0.00	16.67 $\pm$ 0.58	18.33 $\pm$ 0.58	17.33 $\pm$ 0.58
<i>P. aeruginosa</i>	00.00 $\pm$ 0.00	14.33 $\pm$ 0.58	15.33 $\pm$ 0.58	15.67 $\pm$ 0.58
<i>S. aureus</i>	00.00 $\pm$ 0.00	16.33 $\pm$ 0.58	16.67 $\pm$ 0.58	19.33 $\pm$ 0.58
<i>A. baumannii</i>	00.00 $\pm$ 0.00	15.67 $\pm$ 0.58	17.67 $\pm$ 0.58	19.33 $\pm$ 0.58
<i>E. faecalis</i>	00.00 $\pm$ 0.00	17.33 $\pm$ 0.58	18.33 $\pm$ 0.00	16.33 $\pm$ 5.51

**TABLE 3: MIC<sub>90</sub> AND MBC VALUES OF Au, Ag AND Au-Ag ALLOY NPs AGAINST PATHOGENIC *K. pneumoniae* STRAINS**

Test Samples	Au NPs		Ag NPs		Au-Ag NPs	
	<sup>1</sup> MIC <sub>90</sub>	<sup>2</sup> MBC	<sup>1</sup> MIC <sub>90</sub>	<sup>2</sup> MBC	<sup>1</sup> MIC <sub>90</sub>	<sup>2</sup> MBC
Concentration ( $\mu$ g/ml)						
<i>K. pneumoniae</i>	108 $\pm$ 0.00	3ND	64 $\pm$ 0.00	88 $\pm$ 0.00	62 $\pm$ 5.20	80 $\pm$ 0.00
<i>E. coli</i>	108 $\pm$ 0.00	ND	64 $\pm$ 0.00	88 $\pm$ 0.00	61.33 $\pm$ 4.62	88 $\pm$ 0.00
<i>P. aeruginosa</i>	114 $\pm$ 0.00	ND	61.33 $\pm$ 4.62	93.33 $\pm$ 4.62	61.33 $\pm$ 4.62	93.33 $\pm$ 4.62
<i>S. aureus</i>	112 $\pm$ 3.46	ND	61.33 $\pm$ 4.62	85.33 $\pm$ 4.62	53.33 $\pm$ 4.62	77.33 $\pm$ 4.62
<i>A. baumannii</i>	104 $\pm$ 3.46	ND	61.33 $\pm$ 4.62	93.33 $\pm$ 4.62	56 $\pm$ 0.00	77.33 $\pm$ 4.62
<i>E. faecalis</i>	108 $\pm$ 0.00	ND	64 $\pm$ 0.00	88 $\pm$ 0.00	56 $\pm$ 0.00	82.67 $\pm$ 4.62

Note: <sup>1</sup>The concentration that inhibits 90 % (MIC<sub>90</sub>) of bacterial cells, minimum inhibitory concentration; <sup>2</sup>Minimum bactericidal concentration and <sup>3</sup>ND: Not Detected

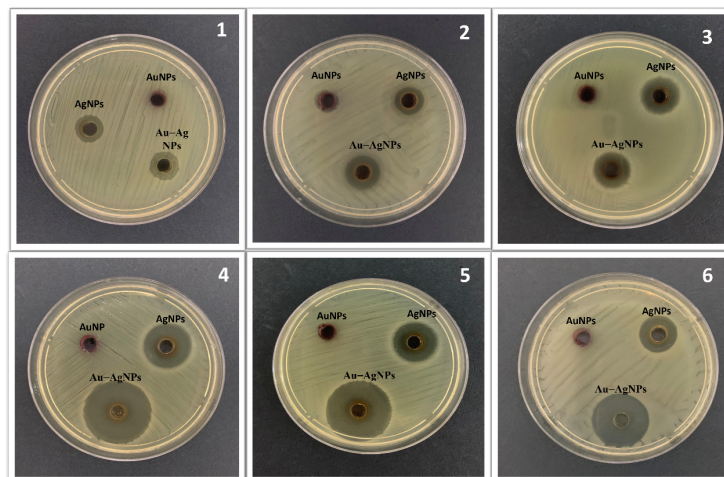


**Fig. 9:** Activity of AgNPs against, (1) *K. pneumoniae*; (2) *E. coli*; (3) *P. aeruginosa*; (4) *S. aureus*; (5) *A. baumannii* and (6) *E. faecalis*

The antimicrobial activity of NPs was investigated against MDR pathogenic *K. pneumoniae*, *E. coli*, *P. aeruginosa*, *S. aureus*, *A. baumannii*, *E. faecalis* strains using agar disk diffusion and microdilution plate methods. *E. faecalis* was found to have the largest ZIN (17.33 mm) of the AgNPs, while *P. aeruginosa* was found to have the minor ZIN (14.33 mm). There was a range of 61.33 to 64 µg/ml of MIC and 85.33 to 93.33 µg/ml of MBC for AgNPs against MDR bacteria. Data from this study agree with those found by Jyoti *et al.*<sup>[53]</sup>. In this study, synthesized AuNPs had no ZIN, indicating that AuNPs have no adverse effect on MDR bacteria. MIC of AuNPs was in high concentration against MDR was not bactericidal. The highest MIC of AuNPs was 114 mg/ml against *P. aeruginosa* strains. Finally, the ZIN of Au-Ag alloy NPs was found to be highest (18.33 mm) against *E. coli* and *E. faecalis* and lowest (15.33 mm) against *P. aeruginosa*, the MIC ranged from 53.33 to 62 µg/ml and the MBC of the Au-Ag alloy NPs ranged from 77.33 to 93.33 µg/ml against MDR strains.

In our results, biosynthesis AgNPs showed an antibacterial effect against MDR bacteria (*E. coli*, *S. aureus*, Methicillin-Resistant *S. aureus* (MRSA), *A. baumannii*, *P. aeruginosa*, *E. faecalis*, *K. pneumoniae*). Previous studies that looked at AgNPs antibacterial activity yielded similar results<sup>[53]</sup>.

The mechanism of the AgNPs inhibitory action on MDR bacteria is still unknown. The small AgNPs synthesized by *Z. spina-christi* leaf extract could explain the antibacterial activity. Sulfur and phosphorus components (proteins and DNA) in the cytoplasm could react with Ag ions released from AgNPs, resulting in a decrease in DNA replication and cell viability. This was confirmed by TEM analysis of cell membrane rupture, which showed that small AgNPs with an extensive

surface area provided larger NPs which have better contact and interaction with bacteria. The thiol group of enzymes, such as Nicotinamide Adenine Dinucleotide Hydrogen (reduced) (NADH) dehydrogenases, could interact with Ag ions and disrupt the respiratory chain. AgNPs also generated free radicals, which oxidized cells and caused cell death<sup>[54,55]</sup>.

In this study, AuNPs showed no ZIN against test MDR bacteria and fragile antibacterial activity at a high concentration of AuNPs<sup>[56]</sup>. However, researchers have found that AuNPs are ineffective or only mildly bactericidal at high concentrations. Furthermore, an efficient drug delivery/carrier system based on AuNPs with specific physicochemical properties has been widely accepted because of their simple and well-studied syntheses, ease of surface functionalization and biocompatibility and low toxicity<sup>[57]</sup>.

Functionalized phytochemicals because of the combination of plant extract, Au and Ag metals, Au-Ag alloy NPs have a more significant ZIN than AuNPs and AgNPs alone<sup>[38]</sup>. A previous study<sup>[58]</sup> discovered that Au-Ag alloy NPs have a larger ZIN than AuNPs and AgNPs alone.

In conclusion, this research suggests a new approach to dealing with MDR bacteria-related infections using *Z. spina-christi* leaves extract, a green strategy for the rapid biosynthesis of Au, Ag and Au-Ag alloy NPs has been developed. This extract contained reducing, stabilizing and capping agents for the biosynthesis of NPs containing Au, Ag and Au-Ag alloy. A UV-Vis spectroscopy analysis showed that NPs formed at 413 nm for AgNPs, 545 nm for AuNPs and 425 nm for the Ag-Au alloy. The XRD analysis confirmed that the synthesized Au, Ag and Au-Ag alloy NPs were Face-Centered Cubic (FCC) phases. Under optimum

conditions, the particles are spherical and hexagonal and have a narrow size distribution with 11.9-40.62 nm diameters.

Furthermore, higher Gram-negative and Gram-positive bacterial growth inhibition biological potential compared to Au, Ag and Au-Ag alloy NPs. In conclusion, Au, Ag and Au-Ag alloy NPs prepared using the environmentally friendly and cost-effective method described here have been predicted to be potential antioxidants, antimicrobials and anticancer agents. In addition, the use of phytochemically functionalized MNPs could result in significant advances in a variety of material science and biology fields.

### Acknowledgements:

The authors thank the Science and Technology Unit, the Deanship of Scientific Research and the Deanship of Graduate Studies at King Abdulaziz University (KAU) in Jeddah, Saudi Arabia, as well as the Department of Biological Sciences for its support and the Department of Biotechnology, Faculty of Science, Taif University, Taif, Kingdom of Saudi Arabia.

### Conflict of interests:

The authors declared no conflict of interest.

### REFERENCES

- Singh P, Kim YJ, Zhang D, Yang DC. Biological synthesis of nanoparticles from plants and microorganisms. *Trends Biotechnol* 2016;34(7):588-99.
- Park TJ, Lee KG, Lee SY. Advances in microbial biosynthesis of metal nanoparticles. *Appl Microbiol Biotechnol* 2016;100(2):521-34.
- Fernandes IJ, Aroche AF, Schuck A, Lamberty P, Peter CR, Hasenkamp W, *et al.* Silver nanoparticle conductive inks: Synthesis, characterization, and fabrication of inkjet-printed flexible electrodes. *Sci Rep* 2020;10(1):1-11.
- Chen X, Schluesener HJ. Nanosilver: A nanoparticle in medical application. *Toxicol Lett* 2008;176(1):1-2.
- Devi P, Patil SD, Jeevanandam P, Navani NK, Singla ML. Synthesis, characterization and bactericidal activity of silica/silver core-shell nanoparticles. *J Mater Sci Mater Med* 2014;25(5):1267-73.
- Morones JR, Elechiguerra JL, Camacho A, Holt K, Kouri JB, Ramirez JT, *et al.* The bactericidal effect of silver nanoparticles. *Nanotechnology* 2005;16(10):2346.
- Vassallo A, Silletti MF, Faraone I, Milella L. Nanoparticulate antibiotic systems as antibacterial agents and antibiotic delivery platforms to fight infections. *J Nanomater* 2020;2020:1-31.
- Cui Y, Zhao Y, Tian Y, Zhang W, Lü X, Jiang X. The molecular mechanism of action of bactericidal gold nanoparticles on *Escherichia coli*. *Biomaterials* 2012;33(7):2327-33.
- Singh AK, Xu Q. Synergistic catalysis over bimetallic alloy nanoparticles. *ChemCatChem* 2013;5(3):652-76.
- Mandal R, Baranwal A, Srivastava A, Chandra P. Evolving trends in bio/chemical sensor fabrication incorporating bimetallic nanoparticles. *Biosens Bioelectron* 2018;117:546-61.
- Grade S, Eberhard J, Jakobi J, Winkel A, Stiesch M, Barcikowski S. Alloying colloidal silver nanoparticles with gold disproportionally controls antibacterial and toxic effects. *Gold Bull* 2014;47(1):83-93.
- Dos Santos MM, Queiroz MJ, Baptista PV. Enhancement of antibiotic effect *via* gold: Silver-alloy nanoparticles. *J Nanopart Res* 2012;14(5):1-8.
- Asiya SI, Pal K, Kralj S, El-Sayyad GS, de Souza FG, Narayanan T. Sustainable preparation of gold nanoparticles *via* green chemistry approach for biogenic applications. *Mater Today Chem* 2020;17:100327.
- Correa-Llantén DN, Muñoz-Ibacache SA, Castro ME, Muñoz PA, Blamey JM. Gold nanoparticles synthesized by *Geobacillus* sp. strain ID17 a thermophilic bacterium isolated from Deception Island, Antarctica. *Microb Cell Fact* 2013;12(1):1-6.
- Maria BS, Devadiga A, Shetty Kodialbail V, Saidutta MB. Synthesis of silver nanoparticles using medicinal *Zizyphus xylopyrus* bark extract. *Appl Nanosci* 2015;5(6):755-62.
- Baptista PV, McCusker MP, Carvalho A, Ferreira DA, Mohan NM, Martins M, *et al.* Nano-strategies to fight multidrug resistant bacteria-“A Battle of the Titans”. *Front Microbiol* 2018;9:1441.
- Hidron AI, Edwards JR, Patel J, Horan TC, Sievert DM, Pollock DA, *et al.* Antimicrobial-resistant pathogens associated with healthcare-associated infections: Annual summary of data reported to the National Healthcare Safety Network at the Centers for Disease Control and Prevention, 2006-2007. *Infect Control Hosp Epidemiol* 2008;29(11):996-1011.
- Klemm EJ, Wong VK, Dougan G. Emergence of dominant multidrug-resistant bacterial clades: Lessons from history and whole-genome sequencing. *Proc Natl Acad Sci USA* 2018;115(51):12872-7.
- Chung IM, Park I, Seung-Hyun K, Thiruvengadam M, Rajakumar G. Plant-mediated synthesis of silver nanoparticles: Their characteristic properties and therapeutic applications. *Nanoscale Res Lett* 2016;11(1):1-4.
- Lee SY, Krishnamurthy S, Cho CW, Yun YS. Biosynthesis of gold nanoparticles using *Ocimum sanctum* extracts by solvents with different polarity. *ACS Sustain Chem Eng* 2016;4(5):2651-9.
- Zhang G, Du M, Li Q, Li X, Huang J, Jiang X, *et al.* Green synthesis of Au-Ag alloy nanoparticles using *Cacumen platycladi* extract. *RSC Adv* 2013;3(6):1878-84.
- Burygin GL, Khlebtsov BN, Shantrokha AN, Dykman LA, Bogatyrev VA, Khlebtsov NG. On the enhanced antibacterial activity of antibiotics mixed with gold nanoparticles. *Nanoscale Res Lett* 2009;4(8):794-801.
- Ahmed S, Saifullah, Ahmad M, Swami BL, Ikram S. Green synthesis of silver nanoparticles using *Azadirachta indica* aqueous leaf extract. *J Radiat Res Appl Sci* 2016;9(1):1-7.
- Ramya Juliet M, Priyanka Beulah GR, Tresina PS, Doss A, Mohan VR. Biogenic synthesis of copper nanoparticles using aquatic pteridophyte *Marsilea quadrifolia* Linn. rhizome and its antibacterial activity. *Int J Nanodimens* 2020;11(4):337-45.
- Panigrahi T. Synthesis and characterization of silver nanoparticles using leaf extract of *Azadirachta indica* (Doctoral dissertation); 2013:1-69.
- Bergey DH, Holt, JG. Bergey's manual of determinative bacteriology. 9<sup>th</sup> ed. Baltimore, USA: Williams and Wilkins; 1994.
- CLSI. Performance standards for antimicrobial disk susceptibility tests, Approved standard M02-A11. 11<sup>th</sup> ed. Wayne, Pennsylvania: National Committee for Clinical Laboratory Standards Institute, CLSI; 2012.
- Greenwood D, Slack RC, Barer MR, Irving WL. Medical Microbiology E-Book: A Guide to Microbial Infections: Pathogenesis, Immunity, Laboratory Diagnosis and Control. With Student Consult Online Access: Elsevier Health Sciences; 2012.

29. Papich MG. Antimicrobials, susceptibility testing and minimum inhibitory concentrations (MIC) in veterinary infection treatment. *Vet Clin Small Anim Pract* 2013;43(5):1079-89.
30. Balouiri M, Sadiki M, Ibsouda SK. Methods for *in vitro* evaluating antimicrobial activity: A review. *J Pharm Anal* 2016;6(2):71-9.
31. SP V, Udayabhanu U, Lalithamba HS. Plant-mediated green synthesis of Ag nanoparticles using *Rauvolfia tetraphylla* (L) flower extracts: Characterization, biological activities and screening of the catalytic activity in formylation reaction. *Sci Iran* 2020;27(6):3353-66.
32. Verma A, Mehata MS. Controllable synthesis of silver nanoparticles using Neem leaves and their antimicrobial activity. *J Radiat Res Appl Sci* 2016;9(1):109-15.
33. Khandel P, Shahi SK, Soni DK, Yadav RK, Kanwar L. *Alpinia calcarata*: Potential source for the fabrication of bioactive silver nanoparticles. *Nano Converg* 2018;5(1):1-7.
34. Ismail EH, Khalil MM, Al Seif FA, El-Magdoub F, Bent AN, Rahman A, *et al.* Biosynthesis of gold nanoparticles using extract of grape (*Vitis vinifera*) leaves and seeds. *Prog Nanotechnol Nanomater* 2014;3:1-2.
35. Abdelhalim MA, Mady MM, Ghannam MM. Physical properties of different gold nanoparticles: Ultraviolet-visible and fluorescence measurements. *J Nanomed Nanotechnol* 2012;3(3):178-94.
36. Yallappa S, Manjanna J, Dhananjaya BL. Phytosynthesis of stable Au, Ag and Au-Ag alloy nanoparticles using *J. sambac* leaves extract, and their enhanced antimicrobial activity in presence of organic antimicrobials. *Spectrochim Acta A Mol Biomol Spectrosc* 2015;137:236-43.
37. Guisbiers G, Mendoza-Cruz R, Bazán-Díaz L, Velázquez-Salazar JJ, Mendoza-Perez R, Robledo-Torres JA, *et al.* Electrum, the gold-silver alloy, from the bulk scale to the nanoscale: Synthesis, properties and segregation rules. *ACS Nano* 2016;10(1):188-98.
38. Godipurge SS, Yallappa S, Biradar NJ, Biradar JS, Dhananjaya BL, Hegde G, *et al.* A facile and green strategy for the synthesis of Au, Ag and Au-Ag alloy nanoparticles using aerial parts of *R. hypocrateriformis* extract and their biological evaluation. *Enzyme Microb Technol* 2016;95:174-84.
39. Silveira AP, Bonatto CC, Lopes CA, Rivera LM, Silva LP. Physicochemical characteristics and antibacterial effects of silver nanoparticles produced using the aqueous extract of *Ilex paraguariensis*. *Mater Chem Phys* 2018;216:476-84.
40. Patil MP, Bayaraa E, Subedi P, Padi LL, Tarte NH, Kim GD. Biogenic synthesis, characterization of gold nanoparticles using *Lonicera japonica* and their anticancer activity on HeLa cells. *J Drug Deliv Sci Technol* 2019;51:83-90.
41. Elemike EE, Onwudiwe DC, Fayemi OE, Botha TL. Green synthesis and electrochemistry of Ag, Au, and Ag-Au bimetallic nanoparticles using golden rod (*Solidago canadensis*) leaf extract. *Appl Phys A Mater Sci Process* 2019;125(1):1-2.
42. Khatami M, Pourseyedi S. *Phoenix dactylifera* (date palm) pit aqueous extract mediated novel route for synthesis high stable silver nanoparticles with high antifungal and antibacterial activity. *IET Nanobiotechnol* 2015;9(4):184-90.
43. Ahmad T, Iqbal J, Bustam MA, Irfan M, Asghar HM. A critical review on phytosynthesis of gold nanoparticles: Issues, challenges and future perspectives. *J Clean Prod* 2021;309:127460.
44. Deng Y, Zhao Y, Padilla-Zakour O, Yang G. Polyphenols, antioxidant and antimicrobial activities of leaf and bark extracts of *Solidago canadensis* L. *Ind Crops Prod* 2015;74:803-9.
45. Islam NU, Jalil K, Shahid M, Muhammad N, Rauf A. *Pistacia integerrima* gall extract mediated green synthesis of gold nanoparticles and their biological activities. *Arab J Chem* 2019;12(8):2310-9.
46. Fleury B, Cortes-Huerto R, Taché O, Testard F, Menguy N, Spalla O. Gold nanoparticle internal structure and symmetry probed by unified small-angle X-ray scattering and X-ray diffraction coupled with molecular dynamics analysis. *Nano Lett* 2015;15(9):6088-94.
47. Matsushita M, Janda KD. Histidine kinases as targets for new antimicrobial agents. *Bioorg Med Chem* 2002;10(4):855-67.
48. WHO. Antibiotic resistance: Multi-country public awareness survey. Geneva, Switzerland: World Health Organization; 2015. p. 59.
49. Navon-Venezia S, Kondratyeva K, Carattoli A. *Klebsiella pneumoniae*: A major worldwide source and shuttle for antibiotic resistance. *FEMS Microbiol Rev* 2017;41(3):252-75.
50. Ali A. Antimicrobial resistance pattern of uropathogens isolated from Rafha central hospital, Rafha, Kingdom of Saudi Arabia. *J Pure Appl Microbiol* 2018;12(2):577-86.
51. Gad El-Rab SM, Halawani EM, Alzahrani SS. Biosynthesis of silver nano-drug using *Juniperus excelsa* and its synergistic antibacterial activity against multidrug-resistant bacteria for wound dressing applications. *3 Biotech* 2021;11(6):1-6.
52. Adaimé A, Hajj A, Hallit S, Sarkis DK. Article original/original article. *Liban Med J* 2020;68(3):127.
53. Jyoti K, Baunthiyal M, Singh A. Characterization of silver nanoparticles synthesized using *Urtica dioica* Linn. leaves and their synergistic effects with antibiotics. *J Radiat Res Appl Sci* 2016;9(3):217-27.
54. Singh K, Panghal M, Kadyan S, Chaudhary U, Yadav JP. Green silver nanoparticles of *Phyllanthus amarus*: As an antibacterial agent against multi drug resistant clinical isolates of *Pseudomonas aeruginosa*. *J Nanobiotechnology* 2014;12(1):1-9.
55. Wu J, Kamaly N, Shi J, Zhao L, Xiao Z, Hollett G, *et al.* Development of multinuclear polymeric nanoparticles as robust protein nanocarriers. *Angew Chem Int Ed* 2014;53(34):8975-9.
56. Zhang J, Li C, Zhang X, Huo S, Jin S, An FF, *et al.* *In vivo* tumor-targeted dual-modal fluorescence/CT imaging using a nanoprobe co-loaded with an aggregation-induced emission dye and gold nanoparticles. *Biomaterials* 2015;42:103-11.
57. Ramachandran R, Krishnaraj C, Kumar VK, Harper SL, Kalaichelvan TP, Yun SI. *In vivo* toxicity evaluation of biologically synthesized silver nanoparticles and gold nanoparticles on adult zebrafish: A comparative study. *3 Biotech* 2018;8(10):1-2.
58. Tabrizi NS, Tazikeh M, Shahgholi N. Antibacterial properties of Au-Ag alloy nanoparticles. *Int J Green Nanotechnol* 2012;4(4):489-94.

This is an open access article distributed under the terms of the Creative Commons Attribution-NonCommercial-ShareAlike 3.0 License, which allows others to remix, tweak, and build upon the work non-commercially, as long as the author is credited and the new creations are licensed under the identical terms

This article was originally published in a special issue, "Modern Applications in Biomedical Research and Pharmaceutical Sciences" *Indian J Pharm Sci* 2022;84(3) Spl Issue "42-53"